Biochemistry

 Volume 36, Number 49 December 9, 1997

Accelerated Publications

Entropic Exclusion by Neurofilament Sidearms: A Mechanism for Maintaining Interfilament Spacing†

Henry G. Brown and Jan H. Hoh*

Departments of Pathology and Physiology, Johns Hopkins University School of Medicine, 725 N. Wolfe Street, Baltimore, Maryland 21205

Received September 3, 1997; Revised Manuscript Received September 29, 1997[⊗]

ABSTRACT: A long-range repulsive force near isolated neurofilaments was detected by exclusion of large molecules and by direct force measurements with atomic force microscopy. Adsorption of isolated native neurofilaments to a solid substrate in a high-salt solution (170 mM NaCl), in the presence of coisolating contaminants, shows that the contaminants are excluded from a zone that extends 50−100 nm from the core of the filament. Force−distance measurements by AFM show the presence of a weak repulsive force that extends >50 nm from the core of the filament; this repulsive force is absent in homopolymers of neurofilament L or trypsinized native filaments that lack the long sidearms present in native filaments. These results suggest that neurofilament sidearms form an entropic brush, thereby providing a mechanism for maintaining interfilament spacing.

Neurofilaments are major cytoskeletal components that play a key role in determining axonal diameter (*1*−*4*). Cross-sections of motor neuron axons show that filaments fill the bore of the axon, with a typical interfilament spacing in the range of 40−60 nm (*4*−*6*). Physical or chemical injuries that alter the local physiologic milieu or disrupt axonal transport create accumulations of densely packed neurofilaments (*7*−*9*). Accumulations also form in transgenic animals with neurofilament overexpression or mutations, changes that disrupt normal filament stoichiometry or assembly (*10*−*14*). These accumulations generally recapitulate processes seen in neurodegenerative diseases such as amyotrophic lateral sclerosis (*15*, *16*), where the accumulations of neurofilaments are thought to be toxic intermediaries of the disease process. Thus, the biological function of neurofilaments is likely to depend on the long-range interactions that maintain a large interfilament spacing.

Neurofilaments, members of the intermediate filament family, are composed of three major polypeptides: NF-L,[1] NF-M, and NF-H (apparent molecular masses 70, 150, and 200 kDa, respectively), with poorly defined stoichiometries within a filament (*17*, *18*). Each neurofilament polypeptide shares homology with other intermediate filaments over a 300 amino acid sequence near the N-terminus, which comprises the filament core. However, unlike other intermediate filament proteins, the C-terminal ends of NF-M and NF-H continue beyond this core region by approximately 300 and 600 amino acids and contain many sites for phosphorylation (*19*−*24*) and glycosylation (*25*, *26*). The

† This work was supported in part by a Cal Ripken/Lou Gehrig Fund for Neuromuscular Research Grant (HGB).

* To whom correspondence should be addressed. Department of Physiology, Johns Hopkins University School of Medicine, 725 N. Wolfe Street, Baltimore, MD 21205. Phone: +1-410-614-3795. Fax: +1-410-614-3797. E-mail: jan.hoh@jhu.edu.

⊗ Abstract published in *Advance ACS Abstracts*, November 1, 1997.

[1] Abbreviations: AFM, atomic force microscopy; ALS, amyotrophic lateral sclerosis; DTT, dithiothreitol; EGTA, ethylene glycoltetraacetic acid; EM, electron microscopy; FV, force volume; HPLC, high pressure liquid chromatography; INN, isolated native neurofilaments; MES, morpholinoethanesulfonic acid; NF, neurofilament; SDS−PAGE, sodium dodecyl sulfate−polyacrylamide gel electrophoresis.

S0006-2960(97)02174-0 CCC: $14.00

neurofilament cores have a diameter of approximately 10−12 nm with a 22 nm axial periodicity, similar to other intermediate filaments (*27*−*29*). In addition, neurofilaments have highly extended sidearms that in rotary shadow electron microscopy project ∼85 nm from the core of the filament. These sidearms are composed of the C-terminal domains of the NF-M and NF-H subunits (*30*−*32*).

The interfilament spacing of neurofilaments appears to involve the long sidearms of NF-M and NF-H (*4*, *30*, *31*, *33*). For example, traumatically induced damage increases neurofilament densities and appears to either collapse the neurofilament sidearms or cause sidearm proteolysis (*9*, *34*, *35*). In addition, transgenic mice that overexpress NF-L show a decrease in interfilament spacing (*14*), possibly due to reduced sidearm density. Two mechanisms to control interfilament spacing based on interactions of long sidearms with neighboring filaments have been put forward. One proposal, based primarily on electron microscopic evidence and the formation of gels of neurofilaments in vitro, is that the sidearms form cross-links between adjacent filaments (*32*, *36*, *37*). The second hypothesis proposes that the high degree of phosphorylation of the sidearms causes an electrostatic repulsion between sidearms (*38*). Here, we present evidence for an additional mechanism: that the thermally driven motion of the sidearms results in an entropic brush that maintains interfilament spacing.

MATERIALS AND METHODS

Purification and Reassembly of Neurofilaments. Neurofilaments were isolated from bovine spinal cord as previously described (*31*). Briefly, diced bovine spinal cord was homogenized with buffer A (100 mM MES, 1.0 mM EGTA, and 0.5 mM $MgCl_2$ at pH 6.5) in a concentration of 10 g of cord/16 mL of buffer. The homogenate was centrifuged at 34500*g* for 30 min at 4 °C. The supernatant was mixed to 30% glycerol and incubated at 37 °C for 20 min. The incubation mix was centrifuged at 158000*g* for 120 min at 20 °C. The pellet was resuspended in buffer C (100 mM MES, 1.0 mM DTT, and 170 mM NaCl at pH 6.5) for imaging as native neurofilaments.

For preparation of homopolymers of NF-L, pellets of native filaments were disassembled in buffer B (6 M urea, 1.0 mM DTT, 25 mM NaH_2PO_4, and 1.0 mM EGTA at pH 7.5); the subunits were separated by HPLC (Pharmacia Mono-Q HR 5/5) with a linear gradient of 0.5 M NaCl. SDS−PAGE was used to check the content and purity of the eluate. NF-L homopolymers were reassembled by open dialysis of the purified NF-L subunits against buffer C. SDS−PAGE of the isolated native neurofilament preparations shows the three major subunits and broad range of contaminating proteins. An 11000*g* centrifugation preferentially sediments the filaments, leaving the contaminants in the supernatant.

To examine sidearm-less isolated native neurofilaments, neurofilaments at a concentration of 0.5−2.0 μg/μL were treated with trypsin (2 μg/mL) for 10 min, and Lima Bean trypsin inhibitor (50 μg/mL) was added to arrest digestion (*39*).

Atomic Force Microscopy. A Nanoscope Multimode AFM (IIIa controller; Digital Instruments, Santa Barbara, CA) equipped with a phase extender operating at room temperature was used in all experiments. For fluid tapping, the cantilever holder used a piezo element to drive the entire holder and thereby the cantilever. Several scanners were available, but a J-type scanner with maximal *xy* range of ∼150 μm was used most often. For fluid imaging 85 μm (base to free end) V-shaped silicon nitride cantilevers (F-type microlevers; Park Scientific, Sunnyvale, CA) were used. The tips of these cantilevers were modified by electron beam deposition (*40*). The frequency response spectra of silicon nitride cantilevers in solution are extremely complex; however, we attempted to drive the cantilevers near their natural resonant frequency of 30−35 kHz (in solution). Integral gain and proportional gains were initially ∼0.5, the combination of amplitude and set point was set empirically, and the scan rate was ∼2 Hz. All images were 512 × 512 pixel (16 bit), data was processed using the Nanoscope software, and a set of tools based on the Interactive Data Language (Research Systems Inc, Boulder, CO) developed in our lab.

AFM Force Volumes. Force volumes are 2D arrays of individual force−distance curves collected on a surface. Force volumes used here were typically 128 nm and 64 pixels in each force distance curve and a 64 × 64 array (4096 curves) over a 1 μm × 1 μm area. The single curve scan rate was 4.0 Hz. The trigger threshold was relative to the zero deflection line. The piezo position at the trigger threshold was recorded as relative distance. Details on the force volume data collection are available in Support Note 240 Rev A from Digital Instruments, 112 Robin Hill, Santa Barbara, CA 93117. We used 320 μm (base to free end) V-shaped silicon nitride cantilevers (C-type microlevers; Park Scientific, Sunnyvale, CA). The nominal spring constant for the cantilevers of 0.01 N/m was used to estimate the interaction force. The trigger thresholds were 5 nm (0.05 nN) and 15 nm (0.15 nN).

RESULTS

Atomic force microscopy of isolated native neurofilaments (INN) adsorbed on a mica surface and imaged in an aqueous solution shows a well-defined filament and a rough background. The latter is produced by contaminants that coisolate and coadsorb with the filaments. However, surrounding the filament core, there is a 35−50 nm "exclusion zone" that is flat and does not contain any adsorbed contaminants (Figure 1A). Because the filament is broadened by the AFM tip, the actual zone is likely closer to 90 nm on either side of the core. This exclusion zone remains after a water rinse and air drying of the preparation (not shown). The effect is not seen in images of reassembled NF-L homopolymers adsorbed in the presence of the same contaminants found in the INN preparation (Figure 1B), and mixing of INN and NF-L preparations yields images with a mixture of filaments with and without exclusion zones (Figure 1C). The NF-L homopolymers differ from the INN in that they lack NF-M and NF-H, which both have long carboxy-terminal domains that extend away from the filament core. These protein domains therefore resemble the grafted polymers commonly used to stabilize colloidal suspension by entropic repulsion (*41*, *42*). This suggests that the exclusion of material near the INN filament core could result from the thermally driven motion of the NF-M and NF-H sidearms (Figure 1D). Such exclusion of proteins has been seen for poly(ethylene oxide) copolymers, grafted onto solid supports (*43*, *44*).

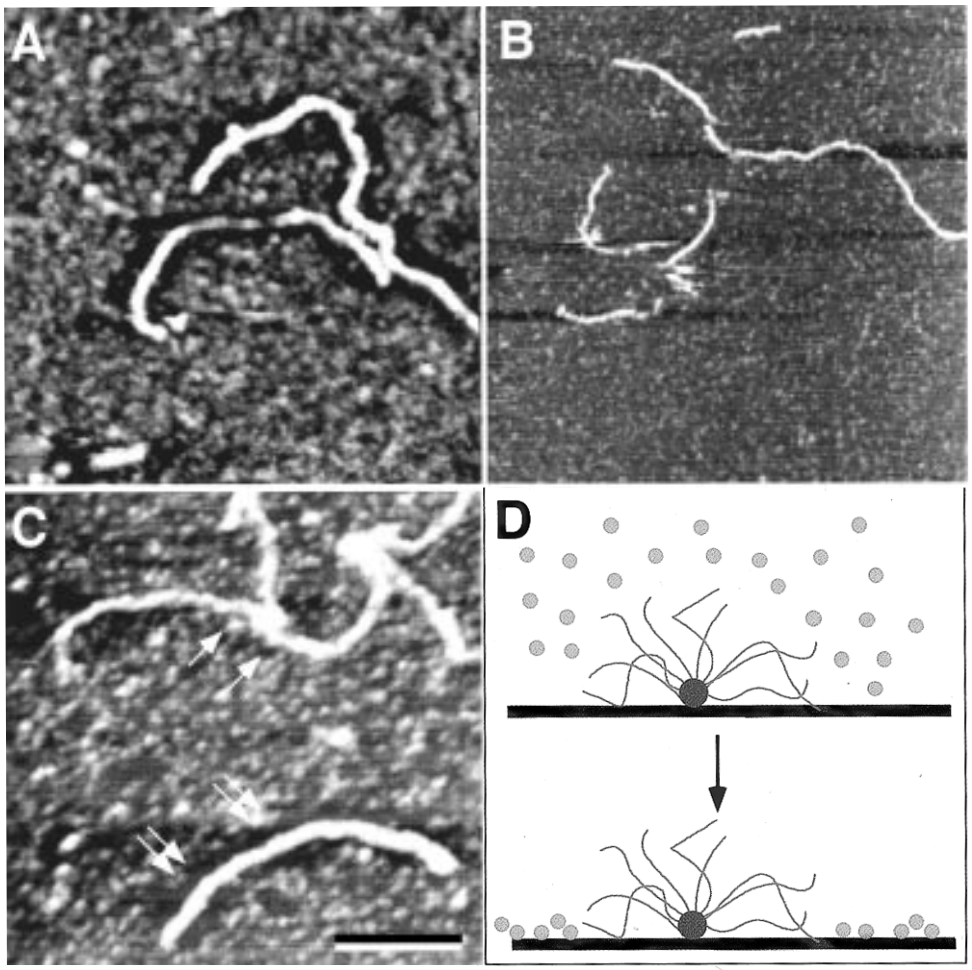

FIGURE 1: AFM image of native neurofilaments and NF-L homopolymers adsorbed to a mica surface (imaged by tapping mode in solution). (A) A 35−50 nm wide exclusion zone around the core of the native neurofilament is clearly visible. The sidearms themselves are not seen, presumably due to their rapid thermal motion. The background material is a mixture of contaminants that coisolate with the neurofilaments. There is some tip broadening, making the core of the native neurofilament appear wider than expected. (B) Homopolymers of NF-L placed in the INN supernantant do not show any exclusion near the core of the filament. The filaments and the background material appear thinner than in panels A or C because the tip is sharper. (C) A mixture of native neurofilament and NF-L filaments shows that some filaments in the preparation have exclusion zones (double arrow), while other filaments lack exclusion zones (single arrow). Scale bar, 500 nm. (D) A schematic showing an interpretation of the adsorption experiment. The neurofilaments adsorb rapidly to the substrate, presumably by electrostatic interactions. The sidearms do not interact strongly with the substrate and move rapidly, driven by thermal energy. During the subsequent adsorption the rapid motion of the sidearms excludes material from the region near the filament core. After adsorption and a rinse to remove material remaining in solution, the adsorbed material around the filament forms the exclusion zone seen in the AFM image.

If the INN sidearms behave like entropic brushes, they should exclude structures that are on the same length scale as the sidearms, and larger. Such a repulsion should act on the AFM tip (radius of curvature at the apex ∼20−50 nm), and thus be detectable in a force−distance curve. Because of the difficulty in placing the tip exactly above a single neurofilament, to make a single force−distance curve, we collected arrays of force curves that covered a large area. These "force volumes" can be used to produce a 2-D map of the force−distance interactions in a given area and can also contain topographic information useful for navigating. By using feedback in the force−distance curves, it is possible to specify a maximum force (trigger threshold) that ends an approach, and retracts the tip. An image of the piezo height (an FV-height image) at the trigger reflects a contour of equal force. A 2D difference map showing the distribution of weak long-range interaction forces is produced by subtracting the FV-height image of a data set collected with a large trigger of 15 nm (0.15 nN) from one with a very small trigger of 5 nm (0.05 nN). Another way of describing this is that the difference maps are produced by subtracting an isoforce image of the surface with the tip in close, hard contact (15 nm trigger) from an isoforce image where the tip is in distant, weak contact (5 nm trigger). The subtraction removes topographic and short-range interactions from the volume, leaving long-range interactions. For INN, these difference maps reveal interaction forces that extend >50 nm above the filaments (Figure 2A). This interpretation of the image is supported by analysis of individual force−distance curves taken from the force volume at positions above the filaments and above the substrate. For NF-L homopolymers co-adsorbed with the supernatent from the INN preparation, the difference maps show very little contrast, and individual force−distance curves show only a weak repulsive interaction that extends to ∼20 nm (Figure 2B). Trypsinization of the INN, which preferentially digests the sidearms compared to the neurofilament core, also reduces the interaction force to a nearly negligible level (Figure 2C).

DISCUSSION

On the basis of the two lines of evidence presented here, exclusion of coisolated material from the proximity of the

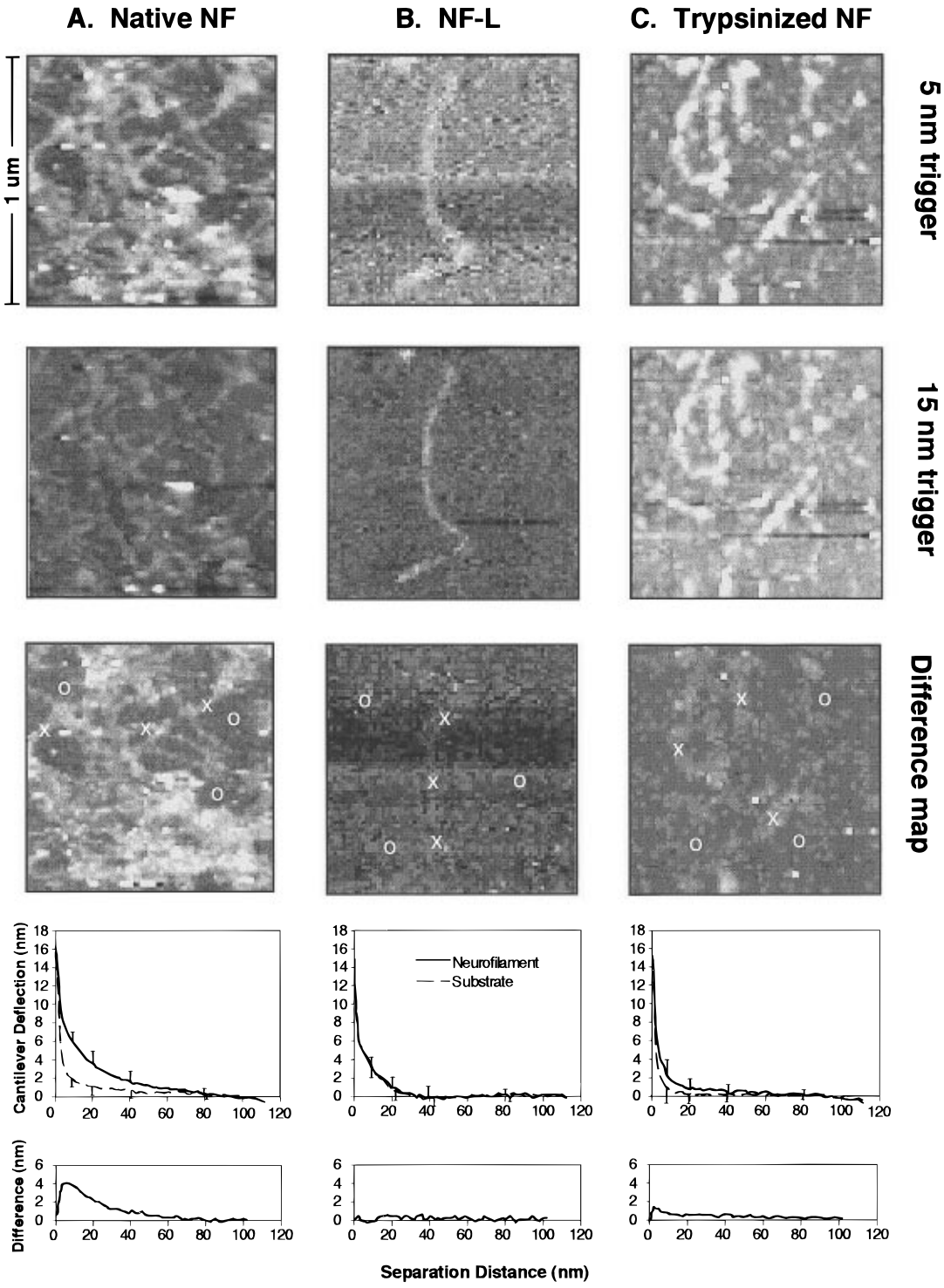

FIGURE 2: Difference maps derived from force volume data sets of native neurofilaments, NF-L homopolymers, and trypsinized native neurofilaments. (A) Isoforce images and a difference map of native neurofilaments, made by substracting an isoforce image at the high deflection trigger (15 nm) from one at the low trigger (5 nm). The difference map shows high contrast between the filaments and the substrate, indicating the presence of forces that act at a distance. Xs and Os mark areas where representative force curves were sampled over neurofilaments and substrate, respectively. Comparing force curves from above the mica substrate ($n = 20$) and above the native neurofilaments ($n = 30$) confirms the presence of the long-range interaction above the neurofilaments. The cantilever deflection over the native neurofilaments begins at a separation distance of >50 nm while the force curves over the substrate do not begin deflection until a separation distance of $\sim$20 nm. The average difference between the force curves collected on a neurofilament and on the mica, which shows the relative magnitude of the force as a function of distance, is shown beneath the force curves. This difference curve is related to the interaction potential, and falls off roughly exponentially with distance. This distance dependence is consistent with Alexander-deGennes theory, in which $F(D) \approx 50LkTs^{-3}e^{[-2\pi(D/L)]}$, where F is the force on the probe tip, k is the Boltzmann constant, T is temperature, L is the brush length, s is the mean distance between polymers on the surface, and D is the separation distance (*41*). (B) Corresponding data for NF-L homopolymers coadsorbed with supernatent from the INN preparation shows essentially no contrast between the filaments and the mica substrate. Force curves taken over NF-L filaments ($n = 16$) do not show cantilever deflection until a separation distance of <20 nm is achieved, similar to the curves over substrate in panel A. (C) Following trypsinization of native neurofilaments, difference map force curves appears essentially identical to those obtained with the NF-L homopolymer.

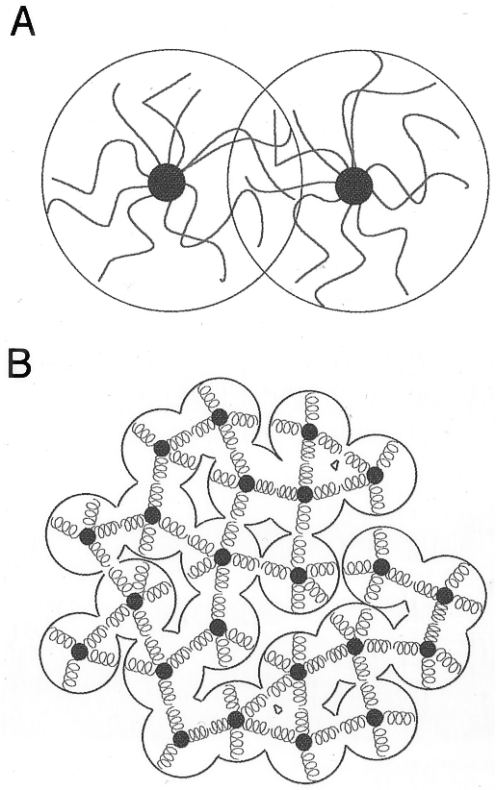

FIGURE 3: Proposed model for entropically controlled interfilament spacing. (A) The thermally driven motion of the sidearms (red) will give each filament an effective volume, depicted by the green circles, much larger than the core of the filament. Two of these volumes interacting would behave as a spring and resist compression (not to scale). (B) Thus, an assembly of neurofilaments (shown schematically in cross section) might be viewed as a collection of tubes separated along their length by entropic springs. These springs would only affect compression, unless tightly bound to an adjacent filament.

neurofilament core, and a repulsive interaction force that extends >50 nm away from the core, we propose that the sidearms of neurofilaments form an entropic brush that is involved in determining the interfilament distance within the axon (Figure 3A). While the sidearms may have some structure dependent stiffness (i.e., enthalpic stiffness), the low density of sidearms per unit length, estimated at 5−10 sidearms per 22 nm by rotary shadow EM (*32*), suggests that a great deal of motion is necessary to produce an exclusion zone of 50−100 nm. Note that the sidearms seen by EM are in projection, and as they extend away from the core of the filament the sidearms become more widely seperated. Simple geometric considerations suggest that at 60 nm away from the core the average distance between sidearms is 28 nm. Neither of the two experiments presented here can be explained solely by electrostatic interactions. The inverse Debye length in 170 mM monovalent salt is on theorder of 0.7 nm, and hence the electrostatic forces become insignificant at distances more than several nanometers away (*41*, *42*); whereas the effects seen here act in the range 10−100 nm. However, electrostatic interactions may play a role in close contacts between the sidearms or the conformation of the sidearms.

There is substantial evidence that neurofilaments are involved in determining axonal bore (*1*−*6*). The results presented here provide a physical mechanism by which the filaments achieve a large effective volume, enabling them to behave as elastic tubes with effective diameters on the order of 100−200 nm. This allows a relatively small number of filaments to fill the axon, while permitting free diffusion of solutes and small molecules. We also suggest that the entropic movement of the neurofilament sidearms underlies a critical role of neurofilaments in the maintenance of axonal bore. Axons extend over large distances and are subject to many forces, including compression; a bundle of neurofilaments separated by entropic "springs" could protect the axon against compression (Figure 3B). Indeed, in response to external compression, neurofilaments form a more ordered cytoskeleton, with interfilament distances decreased to 25 nm from their normal 50 nm (*45*), as might be expected with an increased repulsive force between the filaments. Furthermore, agents or conditions that disturb the behavior of the sidearms, such as increasing their affinity for each other or the filament core, would cause an aggregation of the filaments similar to coagulation or flocculation seen in other colloidal systems (*41*).

ACKNOWLEDGMENT

We thank H. Dintzis, A. Lenhoff, and D. Wirtz for helpful discussions; Y. Liu and E. Hassan, W. Heinz, R. Dumont, and M. Antonik for assistance; J. Troncoso and A. Costello for supplying purified NF-L; Dr. E. Zerhouni for the use of his AFM; and P. Maloney for comments on the manuscripts. We also thank W. Agnew for his ongoing support.

REFERENCES

1. Friede, R. L., and Samorajski, T. (1970) Axon caliber related to neurofilaments and microtubules in sciatic nerve fibers of rats and mice. *Anat. Rec. 167*, 379−387.
2. Hoffman, P. N., Thompson, G. W., Griffin, J. W., and Price, D. L. (1985) Changes in neurofilament transport coincide temporally with alterations in the caliber of axons in regenerating motor fibers. *J. Cell Biol. 101*, 1332−1340.
3. Monaco, S., Autilio-Gambetti, L., Lasek, R. J., Katz, M. J., and Gambetti, P. (1989) Experimental increase of neurofilament transport rate: decreases in neurofilament number and in axon diameter. *J. Neuropathol Exp Neurol. 48*, 23−32.
4. Xu, Z., Marszalek, J. R., and Lee, M. K., Wong, P. C., Folmer, J., Crawford, T. O., Hsieh, S. I., Griffen, J. W., and Cleveland, D. W. (1996) Subunit composition of neurofilaments specifies axonal diameter. *J. Cell Biol. 133*, 1061−9.
5. Lewis, J. C., and Burton, P. R. (1977) Ultrastructural studies of the superior cervical trunk of the mouse: distribution, cytochemistry and stability of fibrous elements in preganglionic fibers. *J. Comp. Neurol. 171*, 605−618.
6. Price, R. L., Paggi, P., Lasek, R. J., and Katz, M. J. (1988) Neurofilaments are spaced randomly in the radial dimension of axons. *J. Neurocytol. 17*, 55−62.
7. Troncoso, J. C., Hoffman, P. N., Griffin, J. W., Hess-Kozlow, K. M., and Price, D. L. (1985) Aluminum intoxication: a disorder of neurofilament transport in motor neurons. *Brain Res. 342*, 172−175.
8. Griffin, J. W., Parhad, I., Gold, B., Price, D. L., Hoffman, P. N., and Fahnestock, K. (1985) Axonal transport of neurofilament proteins in IDPN neurotoxicity. *Neurotoxicology 6*, 43−53.
9. Povlishock, J. T., Marmarou, A., McIntosh, T., Trojanowski, J. Q., and Moroi, J. (1997) Impact acceleration injury in the rat: evidence for focal axolemmal change and related neurofilament sidearm alteration. *J. Neuropathol. Exp. Neurol. 56*, 347−59.
10. Eyer, J., and Peterson, A. (1994) Neurofilament-deficient axons and perikaryal aggregates in viable transgenic mice expressing a neurofilament-beta-galactosidase fusion protein. *Neuron 12*, 389−405.

11. Julien, J. P., Cote, F., and Collard, J. F. (1995) Mice overexpressing the human neurofilament heavy gene as a model of ALS. *Neurobiol. Aging 16*, 487−90; discussion, 490−492.
12. Lee, M. K., Marszalek, J. R., and Cleveland, D. W. (1994) A mutant neurofilament subunit causes massive, selective motor neuron death: implications for the pathogenesis of human motor neuron disease. *Neuron 13*, 975−88.
13. Ohara, O., Gahara, Y., Miyake, T., Teraoke, H., and Kitamura, T. (1993) Neurofilament deficiency in quail caused by nonsense mutation in neurofilament-L gene. *J. Cell Biol. 121*, 387−395.
14. Monteiro, M. J., Hoffman, P. N., Gearhart, J. D., and Cleveland, D. W. (1990) Expression of NF-L in both neuronal and nonneuronal cells of transgenic mice: increased neurofilament density in axons without affecting caliber. *J. Cell Biol. 111*, 1543−57.
15. Julien, J. P. (1995) A role for neurofilaments in the pathogenesis of amyotrophic lateral sclerosis. *Biochem. Cell Biol. 73*, 593−597.
16. Lee, M. K., and Cleveland, D. W. (1996) Neuronal intermediate filaments. *Annu. Rev. Neurosci. 19*, 187−217.
17. Delacourte, A., Filliatreau, G., Boutteau, F., Biserte, G., and Schrevel J. (1980) Study of the 10-nm-filament fraction isolated during the standard microtubule preparation. *Biochem. J. 191*, 543−546.
18. Liem, R. K., and Hutchison, S. B. (1982) Purification of Individual Components of the Neurofilament Triplet: Filament Assembly from the 70 000-Da Subunit. *Biochemistry 21*, 3221−3226.
19. Carden, M. J., Schlaepfer, W. W., and Lee, V. M. (1985) The structure, biochemical properties, and immunogenicity of neurofilament peripheral regions are determined by phosphorylation state. *J. Biol. Chem. 260*, 9805−17.
20. Geisler, N., Vandekerckhove, J., and Weber, K. (1987) Location and sequence characterization of the major phosphorylation sites of the high molecular mass neurofilament proteins M and H. *FEBS Lett. 221*, 403−407.
21. Julien, J. P., and Mushynski, W. E. (1982) Multiple phosphorylation sites in mammalian neurofilament polypeptides. *J. Biol. Chem. 257*, 10467−10470.
22. Lee, V. M., Otvos, L., Jr., Carden, M. J., Hollosi, M., Dietzschold, B., and Lazzarini, R. A. (1988) Identification of the major multiphosphorylation site in mammalian neurofilaments. *Proc. Natl. Acad. Sci. U.S.A. 85*, 1998−2002.
23. Lees, J. F., Shneidman, P. S., Skuntz, S. F., Carden, M. J., and Lazzarini, R. A. (1988) The structure and organization of the human heavy neurofilament subunit (NF-H) and the gene encoding it. *EMBO J. 7*, 1947−1955.
24. Lewis, S. E., and Nixon, R. A. (1988) Multiple phosphorylated variants of the high molecular mass subunit of neurofilaments in axons of retinal cell neurons: characterization and evidence for their differential association with stationary and moving neurofilaments. *J. Cell. Biol. 107*, 2689−2701.
25. Dong, D. L., Xu, Z. S., Chevrier, M. R., Cotter, R. J., Cleveland, D. W., and Hart, G. W. (1993) Glycosylation of mammalian neurofilaments. Localization of multiple O-linked N-acetylglucosamine moieties on neurofilament polypeptides L and M. *J. Biol. Chem. 268*, 16679−16687.
26. Dong, D. L., Xu, Z. S., Hart, G. W., and Cleveland, D. W. (1996) Cytoplasmic O-GlcNAc modification of the head domain and the KSP repeat motif of the neurofilament protein neurofilament-H. *J. Biol. Chem. 271*, 20845−20852.
27. Heins, S., Wong, P. C., Muller, S., Goldie, K., Cleveland, D. W., and Aebi U. (1993) The rod domain of NF-L determines neurofilament architecture, whereas the end domains specify filament assembly and network formation. *J. Cell Biol. 123*, 1517−1533.
28. Hoffman, P. N., and Lasek, R. J. (1975) The slow component of axonal transport. Identification of major structural polypeptides of the axon and their generality among mammalian neurons. *J. Cell Biol. 66*, 351−366.
29. Weber, K., and Geisler, N. (1985) Intermediate filaments: structural conservation and divergence. *Ann. NY Acad. Sci. 455*, 126−143.
30. Gotow, T., Takeda, M., Tanaka, T., and Hashimoto, P. H. (1992) Macromolecular structure of reassembled neurofilaments as revealed by the quick-freeze deep-etch mica method: difference between NF-M and NF-H subunits in their ability to form cross-bridges. *Eur. J. Cell Biol. 58*, 331−345.
31. Troncoso, J. C., March, J. L., Haner, M., and Aebi, U. (1990) Effect of aluminium and other multivalent cations on neurofilaments *in vitro*: an electron microscopic study. *J. Struct. Biol. 103*, 2−12.
32. Hisanaga, S., and Hirokawa, N. (1988) Structure of the peripheral domains of neurofilaments revealed by low angle rotary shadowing. *J. Mol. Biol. 202*, 297−305.
33. Hirokawa, N., Glicksman, M. A., and Willard, M. B. (1984) Organization of mammalian neurofilament polypeptides within the neuronal cytoskeleton. *J. Cell Biol. 98*, 1523−1536.
34. Povlishock, J. T., and Pettus, E. H. (1996) Traumatically induced axonal damage: evidence for enduring changes in axolemmal permeability with associated cytoskeletal change. *Acta Neurochir. 66*, 81−86.
35. Hall, G. F., and Lee, V. M. (1995) Neurofilament sidearm proteolysis is a prominent early effect of axotomy in lamprey giant central neurons. *J. Comp. Neurol. 353*, 38−49.
36. Leterrier, J. F., and Eyer, J. (1987) Properties of highly viscous gels formed by neurofilaments in vitro. A possible consequence of a specific inter-filament cross-bridging. *Biochem. J. 245*, 93−101.
37. Leterrier, J. F., Kas, J., Hartwig, J., Vegners, R., and Janmey, P. A. (1996) Mechanical effects of neurofilament cross-bridges. Modulation by phosphorylation, lipids, and interactions with F-actin. *J. Biol. Chem. 271*, 15687−15694.
38. Carden, M. J., Trojanowski, J. Q., Schlaepfer, W. W., Lee, V. M. (1987) Two-stage expression of neurofilament polypeptides during rat neurogenesis with early establishment of adult phosphorylation patterns. *J. Neurosci. 7*, 3489−3504.
39. Chin, T. K., Eagles, P. A., and Maggs, A. (1983) The proteolytic digestion of ox neurofilaments with trypsin and alpha-chymotrypsin. *Biochem. J. 215*, 239−252.
40. Keller, D. J., and Chou, C. C. (1992) Imaging steep, high structures by scanning force microscopy with electron-beam deposited tips. *Surf. Sci. 268*, (1−3), 333−339.
41. Israelachvili, J. N. (1992) *Intermolecular and surface forces*, 2nd ed., p 460, New York, Academic Press.
42. Hunter, R. J. (1986) *Foundations of colloid science*, 1 Vol., p 673, Oxford.
43. Tan, J. S., and Martic, P. S. (1990) *J. Colloid Interface Sci. 136*, 415.
44. Schroën, C. G. P. H., Cohen, S. M. A., van der Voort, M. K., van der Padt, A., and van't Riet, K. (1995) Influence of preadsorbed block copolymers on protein adsorption: surface properties, layer thickness, and surface coverage. *Langmuir 11*, 3068−3074.
45. Price, R. L., Lasek, R. J., and Katz, M. J. (1993) Neurofilaments assume a less random architecture at nodes and in other regions of axonal compression. *Brain Res. 607*, 125−133.

BI9721748